Historical and future black carbon deposition on the three ice caps: Ice core measurements and model simulations from 1850 to 2100

Susanne E. Bauer,[1,2] Alexandra Bausch,[1] Larissa Nazarenko,[1,2] Kostas Tsigaridis,[1,2] Baiqing Xu,[3] Ross Edwards,[4] Marion Bisiaux,[5] and Joe McConnell[5]

Received 31 January 2013; revised 27 June 2013; accepted 27 June 2013.

[1] Ice core measurements in conjunction with climate model simulations are of tremendous value when examining anthropogenic and natural aerosol loads and their role in past and future climates. Refractory black carbon (BC) records from the Arctic, the Antarctic, and the Himalayas are analyzed using three transient climate simulations performed with the Goddard Institute for Space Studies ModelE. Simulations differ in aerosol schemes (bulk aerosols vs. aerosol microphysics) and ocean couplings (fully coupled vs. prescribed ocean). Regional analyses for past (1850–2005) and future (2005–2100) carbonaceous aerosol simulations focus on the Antarctic, Greenland, and the Himalayas. Measurements from locations in the Antarctic show clean conditions with no detectable trend over the past 150 years. Historical atmospheric deposition of BC and sulfur in Greenland shows strong trends and is primarily influenced by emissions from early twentieth century agricultural and domestic practices. Models fail to reproduce observations of a sharp eightfold BC increase in Greenland at the beginning of the twentieth century that could be due to the only threefold increase in the North American emission inventory. BC deposition in Greenland is about 10 times greater than in Antarctica and 10 times less than in Tibet. The Himalayas show the most complicated transport patterns, due to the complex terrain and dynamical regimes of this region. Projections of future climate based on the four CMIP5 Representative Concentration Pathways indicate further dramatic advances of pollution to the Tibetan Plateau along with decreasing BC deposition fluxes in Greenland and the Antarctic.

Citation: Bauer, S. E., A. Bausch, L. Nazarenko, K. Tsigaridis, B. Xu, R. Edwards, M. Bisiaux, and J. McConnell (2013), Historical and future black carbon deposition on the three ice caps: Ice core measurements and model simulations from 1850 to 2100, *J. Geophys. Res. Atmos.*, *118*, doi:10.1002/jgrd.50612.

1. Introduction

[2] Estimates of climate forcings from aerosol species are poorly quantified at present. In order to inform policymakers about future climate trends from all forcing agents, general circulation models (GCMs) must be validated using past aerosol records [*McConnell*, 2010]. Although long-lived greenhouse gases (GHGs) constitute the foremost driver of climate change, short-lived aerosols remain major contributors to global radiative forcing and can have a warming or cooling effect by either absorbing or reflecting solar radiation, respectively. Short-lived aerosol climate forcers, such as black carbon (BC), remain in the atmosphere for comparably short periods of time (i.e., days for aerosols as opposed to hundreds of years for some GHGs). Therefore, the impacts of BC on climate occur largely on local and regional scales, with BC's residence time being the controlling parameter of its radiative forcing.

[3] In addition to absorbing radiation when lofted in the atmosphere, BC also causes surface warming when deposited on snow and ice surfaces [*Flanner et al.*, 2007; *Hansen and Nazarenko*, 2004]. Sensitive regions (e.g., the Arctic and the Himalayas) are particularly vulnerable to warming due to the snow albedo effect [*Kopacz et al.*, 2011; *McConnell*, 2010], which tends to enhance snow and ice melting due to the absorption caused by the increased BC deposition. Additionally, increases in surface temperature cause perturbations to the duration and timing of the melt season [*Hansen and Nazarenko*, 2004]. Recent developments in ice core analytical techniques yield highly resolved historical records of primary carbonaceous aerosols, both BC and organic carbon (OC), and sulfate [*Bisiaux et al.*, 2012b; *McConnell et al.*, 2007; *Xu et al.*, 2009]. Observational data of BC and OC in

[1]Center for Climate Systems Research, The Earth Institute, Columbia University, New York, New York, USA.
[2]NASA Goddard Institute for Space Studies, New York, New York, USA.
[3]Key Laboratory of Tibetan Environment Changes and Land Surface Processes, Institute of Tibetan Plateau Research, Chinese Academy of Sciences, Beijing, China.
[4]Department of Imaging and Applied Physics, Curtin University, Bentley, Western Australia, Australia.
[5]Desert Research Institute, Reno, Nevada, USA.

Corresponding author: S. E. Bauer, Center for Climate Systems Research, The Earth Institute, Columbia University, Broadway 2880, New York 10025, NY, USA. (Susanne.Bauer@Columbia.edu)

2169-897X/13/10.1002/jgrd.50612

Table 1. Emissions, Loads, Removals, and Residence Times of BC and OC in the Three Different Model Versions for PD (1996–2005) and PI (1880–1889) Conditions[a]

		Emission Biomass	Emission Fuels	Load	Wet Removal	Dry Removal	Residence Time
		(Tg/a)	(Tg/a)	(Tg)	(Tg/a)	(Tg/a)	(days)
				Preindustrial			
BC	MATRIX_AMIP	2.8	1.82	0.049	3.38	1.12	4.0
	TCADI_AMIP			0.064	3.28	1.23	5.2
	TCADI_OCN			0.063	3.28	1.23	5.1
OC	MATRIX_AMIP	34.75	25.6	0.74	43.59	15.29	4.6
	TCADI_AMIP			1.07	41.26	12.62	7.3
	TCADI_OCN			1.12	41.44	18.41	6.8
				Present Day			
BC	MATRIX_AMIP	3.57	5.15	0.09	6.41	2.0	3.9
	TCADI_AMIP			0.14	6.23	2.24	6.0
	TCADI_OCN			0.14	6.22	2.23	6.0
OC	MATRIX_AMIP	44.14	34.59	0.93	57.80	18.80	4.3
	TCADI_AMIP			1.53	59.54	17.73	7.2
	TCADI_OCN			1.56	59.6	17.6	7.4

[a]Dry removal is given as the sum over dry turbulent deposition and gravitational settling.

frozen media can be used to examine potential correlations between primary carbonaceous aerosol deposition and long-term climatic changes.

[4] In the present assessment, we seek to elucidate past and future climate effects caused by carbonaceous aerosols by using recent observations. We evaluate three 150 year long historical climate simulations, one of which is a 250 year long simulation that is extended into the future. All simulations are carried out with the Goddard Institute for Space Studies (GISS) modelE, but the simulations are performed with different ocean couplings and aerosol schemes. Here we want to investigate the following questions: (1) How well can we constrain current BC residence times? (2) How well can we simulate historical concentrations of the past 150 years? (3) What will be the future BC deposition fluxes at the three ice caps following the four CMIP5 RCP future scenarios?

[5] This paper begins with an analysis of BC residence time at present-day climate conditions. The next part discusses the past 150 years by simulating carbonaceous aerosol deposition and comparing to observed values from snow and ice cores in regions where ice core data are available. These regions, namely Antarctica, Greenland, and the Himalayas, have seasonal and permanent snow or ice cover. We subsequently discuss projected future regional responses in snow- and ice-covered regions due to BC aerosol deposition and then finish the paper with conclusions and perspectives. The technical details about the climate model simulations are given in Appendix A.

2. BC Residence Time Under Present-Day Conditions

[6] Prior to analyzing the historical time series at remote locations, we want to understand how the three model BC simulations differ under present-day conditions. The model simulations, all of which are run as five-member ensembles (see Appendix A2), differ in their ocean couplings and aerosol schemes (as described in Appendix A1). We will use the following abbreviations: TCADI_OCN is the bulk aerosol scheme coupled to the dynamical ocean, TCADI_AMIP uses a prescribed ocean, and MATRIX_AMIP uses the microphysical aerosol scheme and the prescribed ocean.

2.1. Residence Time

[7] The residence time of individual aerosol particles varies greatly in space and time. Some particles get removed close to their point of emission while others may be transported large distances before they are removed. The mean residence time

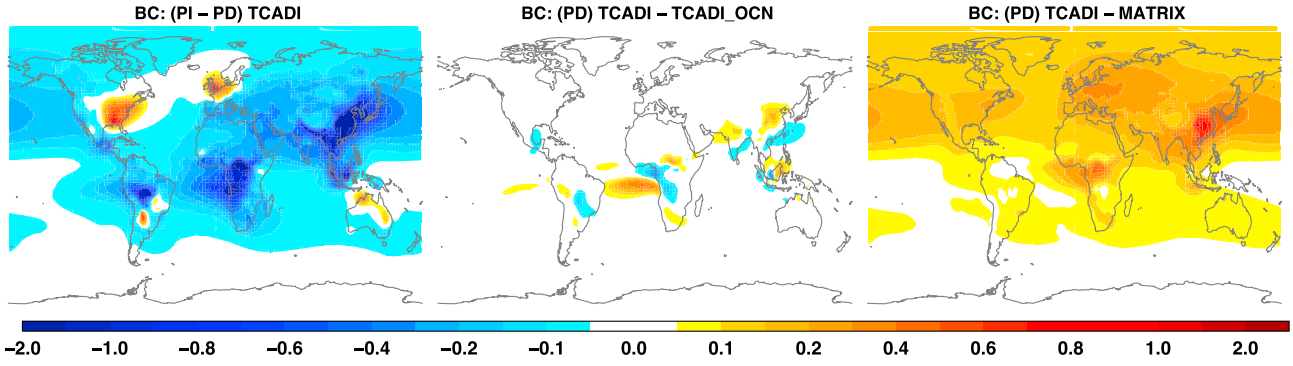

Figure 1. Differences in black carbon mass loads (g/m^2). Differences are shown (left) for preindustrial (1880–1889) and present-day (1996–2005) conditions, (middle) for present-day condition between the coupled ocean and prescribed ocean run (TCADI_AMIP-TCADI_OCN), and (right) for the two different aerosol physics schemes (TCADI_AMIP-MATRIX_AMIP).

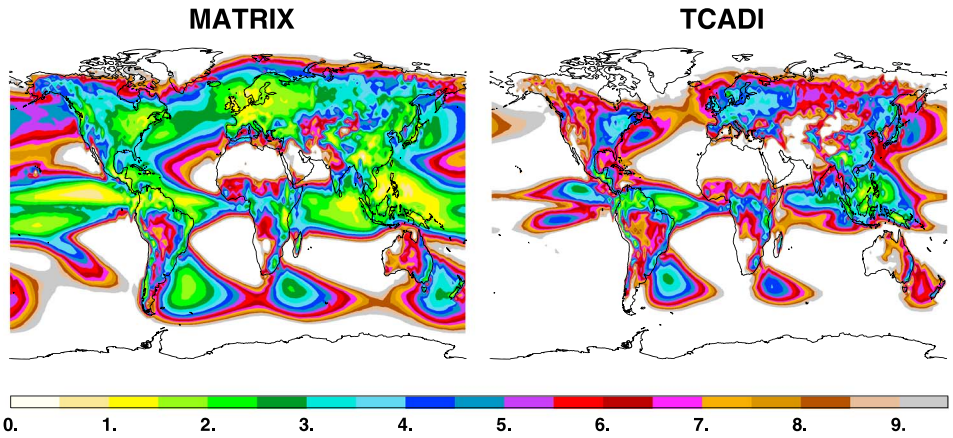

Figure 2. Black carbon residence times as simulated for present-day conditions with (left) MATRIX_AMIP and (right) TCADI_AMIP. Units are in days.

of aerosol species informs us on average how long a particle stays in the atmosphere before it is removed. The residence time of a species is determined by dividing the total load of the species by its removal rates. $\tau_i = L_i/(R_{wet\ i} + R_{dry\ i} + R_{gs\ i})$, where τ is the residence time (days), L the load (kg/m^2), and R the removal rates (kg/m^2/days) of gravitational settling, dry and wet deposition. In this modeling example, we can explain the differences in BC concentrations between TCADI_AMP and MATRIX_AMIP solely by their removal rates, because emission fluxes are identical in all simulations.

[8] Table 1 and Figure 1 (right panel) show that TCADI_AMIP has higher BC loads than MATRIX_AMIP, caused by longer residence times, $\tau_{BC} = 6$ for Tracers, Chemistry, Aerosols, Direct And Indirect Effects (TCADI) and $\tau_{BC} = 3.9$ days for Multiconfiguration Aerosol Tracker Of Mixing State (MATRIX). A map of residence times is given in Figure 2, demonstrating that the shortest residence times are calculated in source regions and regions with large rain rates. Wet removal is 3 times more efficient in removing BC from the atmosphere in the model compared to dry deposition processes. Precipitation rates and distributions are very similar in TCADI_AMIP and MATRIX_AMIP, caused by prescribed ocean temperatures and the absence of the second indirect effect from the calculations.

[9] It is always a challenge to evaluate global models with limited data sets, but here we aim to examine near-source surface measurements, vertical profile measurements over the Pacific, and deposition flux measurements at remote locations. The North American Interagency Monitoring of Protected Visual Environments (IMPROVE) network provides the most data points for surface BC observations but only covers the United States. The IMPROVE network collects surface data sets primarily in remote locations. Particles collected at these sites have undergone processing but to a lesser extent than at the mid-Pacific (HIPPO) or arctic locations. Figure 3 shows measured and modeled BC near-surface concentrations as averaged over 177 stations. Models and observations agree well, with annual mean BC concentrations of 0.21 (IMPROVE), 0.20 (MATRIX_AMIP), and 0.22 µg/m^3 (TCADI_AMIP and TCADI_OCN).

[10] The HIPPO campaign [*Schwarz et al.*, 2010] conducted nearly pole-to-pole profile measurements of trace gases during all seasons from 2009 to 2011. Flight tracks of HIPPO campaigns 1 to 5 are used for this comparison. The flights covered some parts of the United States but mostly probed air over the mid-Pacific. Figure 4 presents a comparison between observed and modeled BC mixing ratios by interpolating the modeled data onto the flight track and using the modeled monthly mean concentrations appropriate for the observed month. MATRIX agrees very well with the observations in the lowest 2 km but underestimates BC mixing ratios above. TCADI shows overly high BC concentrations throughout the entire column.

[11] An even more remote point of reference can be obtained from the present-day concentrations of the ice core measurements (Figures 6, 9, and 10). We will discuss this in more detail in the next section, but in general, we find MATRIX to have lower concentrations than TCADI runs, while for present-day conditions, MATRIX is in better agreement with the ice core data. However, the concentration differences at the remote locations are small.

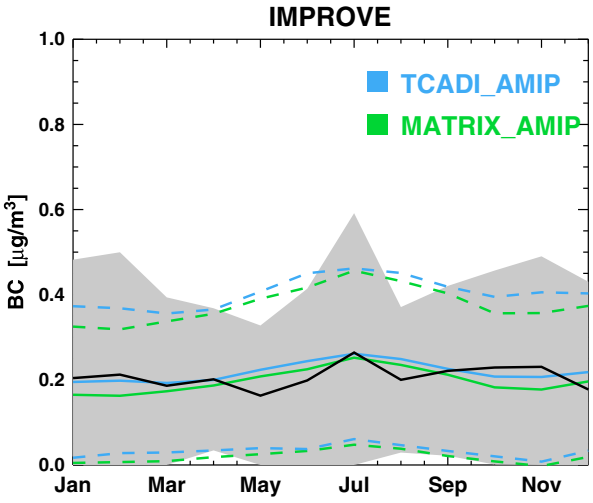

Figure 3. Near-surface BC concentrations for the year 2008 are averaged over 177 IMPROVE stations. Observations are shown in black and standard deviations in grey. Model results are presented for TCADI_AMIP (blue) and MATRIX_AMIP (green). Dashed lines show standard deviations. Units are (µg/m^3).

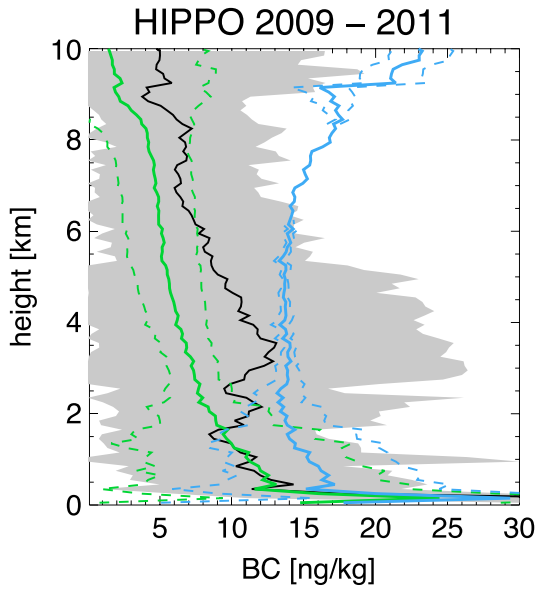

Figure 4. BC mixing ratio profiles (ng/kg) from HIPPO observations (black and standard deviations in grey) and modeled profiles: TCADI_AMIP (blue) and MATRIX_AMIP (green). Dashed lines show standard deviations. Data are averaged over 787 vertical profiles observed during HIPPO 1 to 5.

[12] The conclusions we can draw from the present-day evaluation are biased by the temporal and spatial availability of the observations. The near-source observations discussed here only cover the United States. Therefore, we cannot make judgments on how model performance is affected by emissions in the rest of the world. HIPPO is limited to a few days of observations yet provides the unique opportunity to investigate the vertical distribution of BC at remote locations, which are influenced by individual weather conditions and emission events that are not matched by climate simulations. Models can be used to study campaign events by using daily fire emissions (the climate simulations here use decadal emission information) and nudged meteorology. However, this work is not a subject of this paper.

[13] Removal processes cause the differences in BC concentrations between the MATRIX and TCADI models. Insoluble BC would only appear in MATRIX if particles have not been exposed to other particles or condensates. However, due to fast mixing processes and the fact that most emissions are coemitted with other species, insoluble BC becomes nonexistent within a few hours after emission time. The differences between the models' vertical BC concentrations are caused by the solubility and cloud activation assumptions (see Appendix A). MATRIX's highly soluble BC particles get scavenged more efficiently compared to TCADI's BC. Proportional larger concentrations of TCADI's BC are then entrained into convective updrafts, leading to higher concentrations in the free troposphere. It is of note that, since the CMIP5 simulations, we have improved the entrainment rate parameterizations (though no transient climate simulations have been performed yet), which prevent the accumulation of BC in the upper troposphere in TCADI. MATRIX BC does not react as strongly to the entrainment settings due to the generally stronger wet removal.

[14] Overall, the residence time of BC is influenced by its microphysical properties, transport, and in-cloud and turbulent removal processes. Further sensitivity experiments and cleverly designed observational studies are necessary to distinguish removal from transport features. Nevertheless, we can conclude that the shorter residence times of about 4 days in MATRIX fit better with observations when using the CMIP5 emission inventory.

2.2. Ocean Coupling

[15] The ocean coupling can impact BC concentrations via dynamical differences that are introduced by sea surface temperature variations between the simulations. The differences for BC between the two ocean coupled runs, TCADI_OCN and TCADI_AMIP, are small (Table 1). The global mean load, removal, and residence time change only slightly. The BC load (Figure 1, middle panel) differences in the equatorial region are caused by a shift of the Intertropical Convergence Zone (ITCZ) that changes the circulation and precipitation patterns and thus the aerosol transport and removal in that area. Precipitation patterns between TCADI and MATRIX are very similar in the AMIP simulation.

[16] Both AMIP models overestimate global mean precipitation rates relative to the Climate Prediction Center Merged Analysis of Precipitation (CMAP) data set http://www.esrl.noaa.gov/psd/data/gridded/data.cmap.html. The 1995–2005 mean in CMAP is 2.6 mm/day and 3.1 mm/day in the TCADI_AMIP and TCADI_OCN models. In an absolute sense, the model biases are most pronounced over the tropical Atlantic and Pacific; elsewhere, the agreement between CMAP and TCADI_AMIP is better with biases below 1 mm/day. As is common in coupled ocean simulations, rainfall biases in TCADI_OCN are most pronounced in the tropics due to a double ITCZ structure. The skill of TCADI_OCN in the extratropics is not appreciably affected by the pattern of tropical biases. The errors in tropical rain rates and pattern affect BC deposition fluxes in the Himalayan region (as will be further discussed in section 3) but have very little impact on BC's residence time. Thus, the TCADI_OCN and TCADI_AMIP simulations show similar BC concentrations in the polar regions, bolstering the relevance of our coupled ocean experiments to the future scenarios (section 4).

3. Historical Aerosol Deposition Fluxes in Ice Core Records

[17] The ice core records contain information about historical concentration levels of BC at all stations discussed here. Additionally, sulfur and OC measurements are available from the Greenland and Himalayan cores, respectively. In combination with the model simulations, we can test hypotheses on residence time changes, likely emission evolvements and radiative forcings.

3.1. Antarctic

3.1.1. Observed Trends in Ice Core Records

[18] Two refractive black carbon records [*Bisiaux et al.*, 2012a, 2012b], spanning the time period 1850–2001, have been taken in the Antarctic (Figure 5a). The West Antarctic Ice Sheet (WAIS) ice core (79.46°S, 112.08°W, 1766 m above sea level (asl)) represents the most remote location in this study. Ice core BC concentrations for these sites were determined as refractory BC using an ice core melting system coupled to a nebulizer/desolvator and single particle intracavity laser soot

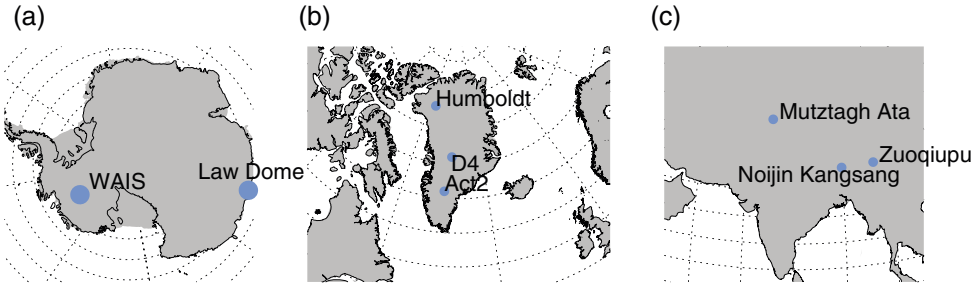

Figure 5. Location of the ice records used in the present study in the (a) Antarctic, (b) Greenland, and (c) the Tibetan Plateau.

photometer (SP2) similar to that of *McConnell et al.* [2007]. Measured BC deposition fluxes (Figure 6a) show values of about 0.01 to 0.02 ng/m^2 with minimal interannual variability and no clear long-term trend. The Law Dome record (66.75°S, 112.37°E, 1230 m asl), separated by ~3500 km from WAIS, shows higher maxima compared to WAIS (Figure 6b). Similar to WAIS, Law Dome is not exposed to local emissions, but due to its coastal location, it is more exposed to long-range transported emissions from the Southern Hemispheric (SH) continents and shipping. The records show large-scale changes in BC deposition linked to climate variability such as the El Niño Southern Oscillation (ENSO) and the anthropogenic modification of fire regimes [*Bisiaux et al.*, 2012a]. Fluctuations in the records from the 1950s to 1980s correlate well with the decadal variability in grassland and biofuel BC emission inventories [*Bisiaux et al.*, 2012b; *Lamarque et al.*, 2010].

3.1.2. Model Simulation

[19] The models simulate that precipitation at the Antarctic stations is always in the form of snow, with simulated average snowfall rates of 0.4 mm/day at WAIS and 1.2 mm/day at Law Dome. The TCADI_OCN model shows a slight increasing trend in snowfall rates reaching ~1.6 mm/day at present day (PD) at Law Dome, whereas the AMIP models show no trend. Antarctic sea ice is retreating too quickly in the TCADI_OCN coupled simulation (G. A. Schmidt et al., in preparation, 2013), which led to increased snowfall rates at Law Dome.

[20] The modeled BC deposition time series (Figure 6) represent the annual mean and ensemble mean of five climate simulations per model. All models overestimate BC deposition rates at both Antarctic stations. Yet deposition values are very low, leading to an actual absolute disagreement that is very small. The models also show an increasing trend from the 1950s onward. Moving the model points 1000 km further inland (dashed lines in Figure 6) removes this trend in MATRIX, but it is still present in TCADI. The strong increase in deposition fluxes in the model simulations after 1960 for the TCADI model is due to the increased lifetime of BC in the TCADI model compared to that of MATRIX. The relative change between natural and energy-related BC sources over the last 150 years has led to an increase in BC residence time from 5 days during preindustrial (PI) times (1850–1860) to 6 days at PD (1995–2005, see Table 1) in the TCADI simulations, whereas physically derived BC residence times in the microphysical model MATRIX stayed at about 4 days throughout the centuries. The comparison demonstrates that residence times between PD and PI periods should not have changed, as simulated by MATRIX. As early as PI times, enough coating materials, such as organics, sulfates, salts, or nitrates, were available to age BC particles quickly.

[21] Based on *Lamarque et al.* [2010], emission fluxes in the SH (Figure 7) are strongly dominated by biomass burning, with more than 90% of the total PI Southern Hemispheric emissions coming from biomass burning. Emissions from all sources tend to increase after 1950, especially from biomass burning in Africa (SH). Anthropogenic emissions show as thoroughly increasing trends, attributed to the domestic sector in Africa and the transportation and industry sector in the SH Americas. The design of the GISS aerosol scheme allows us to examine the aerosol origin. Biomass burning aerosol emissions were the dominating source for BC reaching WAIS in 1880 (Figure 8a) while increasing fossil and biofuel consumption have since made aged industrial BC the dominant source

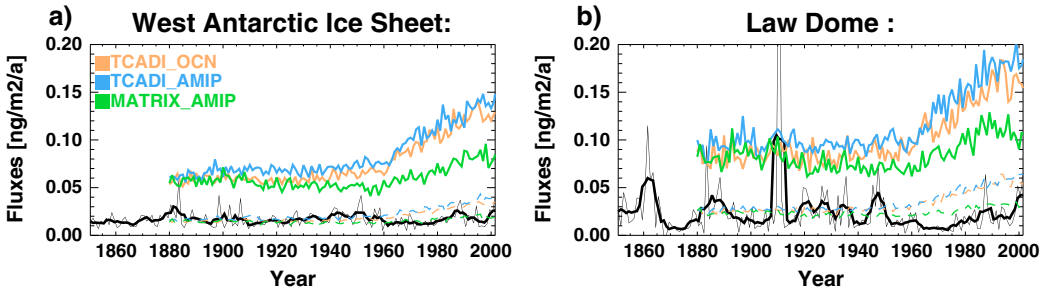

Figure 6. Refractory black carbon deposition fluxes (ng/m^2/a) time series at the (a) Antarctic stations WAIS and (b) Law Dome. Annual (thin line) and 5 year mean (thick line) ice core measurements (black) and model simulations (solid lines): TCADI_OCN (orange), TCADI_AMIP (blue), and MATRIX_AMIP (green). Adjusted model values (dashed lines) are explained in the text.

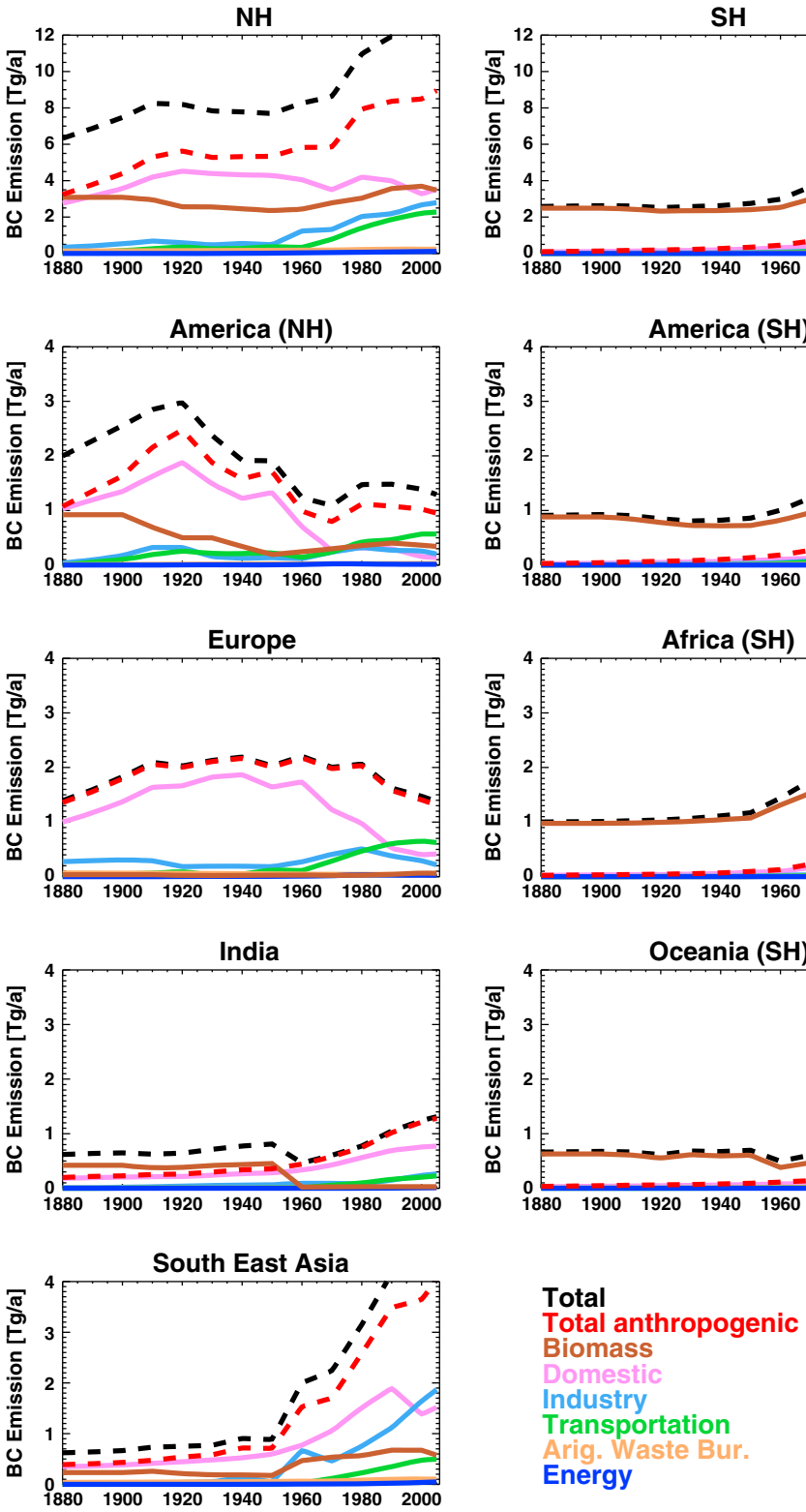

Figure 7. BC emissions from different sectors and regions between 1880 and 2005 [*Lamarque et al.*, 2010].

after 1980. However, the fact that the TCADI models overestimate BC enforces the conclusion that biomass burning and anthropogenic aerosols should have faster aging rates as no increasing trend is visible in the Antarctic ice cores. The overestimated PD BC concentrations in the TCADI models especially point to the overly slow aging process of the anthropogenic BC aerosols.

3.1.3. ENSO Variability

[22] The measured temporal variability in BC deposition at Law Dome has been linked to climate variability [*Bisiaux*

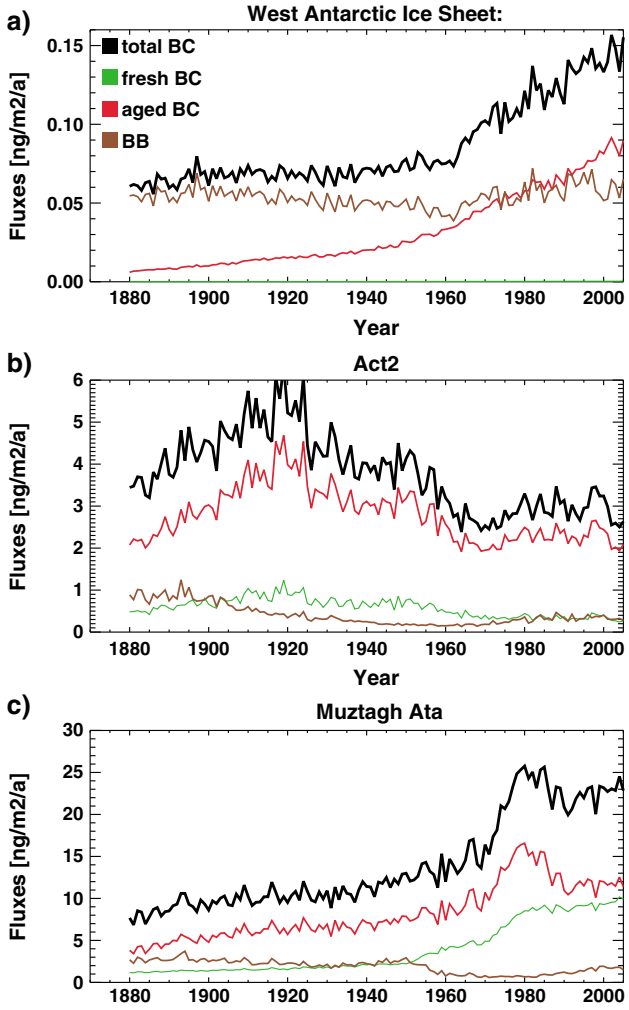

Figure 8. BC deposition fluxes by aerosol type as simulated by TCADI_AMIP. Total BC in black, with aerosol types marked as fresh industrial BC (green), aged industrial BC (red), and biomass burning BC (brown).

et al., 2012a]. The models, however, do not reproduce this pattern. The models' variability is damped by showing the ensemble mean in Figure 6, an average of five similar runs that differ only in their initial conditions (see Appendix A2). However, even in the individual runs (not shown), the large temporal variability seen at Law Dome cannot be reproduced. The two AMIP simulations include ENSO intrinsically, due to the prescribed sea surface temperatures. The fully coupled ocean model (TCADI_OCN) resolves ENSO but with a reduced amplitude. The observed standard deviation of 0.93 K is simulated with 0.85 K in TCADI_OCN (G. A. Schmidt et al., in preparation, 2013). ENSO can influence Southern Hemispheric BC deposition rates via transport and removal changes and, more importantly, via shifts in biomass burning events. The latter is, however, not included in our simulations due to the use of prescribed decadal biomass burning emissions [*Lamarque et al*., 2010] and not the GISS modelE interactive fire module [*Pechony and Shindell*, 2010]. Therefore, we speculate that climate variability influencing biomass burning is most likely the explanation for the observed decadal variability in BC deposition at Law Dome rather than ENSO's influence on transport and removal patterns.

3.2. Greenland

3.2.1. Observed Trends in Ice Core Records

[23] Measurements were made by *McConnell et al*. [2007] on ice cores collected in 2003 from high-snowfall regions in Greenland, specifically at Act2 (66.00°N, 45.12°W, 2408 m asl), D4 (71.42°N, 45.12°W, 2766 m asl), and Humboldt (78.31°N, 56.49°W, 1985 m asl). BC contents in the ice cores were measured with a laser soot photometer SP2, the same method that was used in the Antarctic. BC deposition fluxes varied significantly during the past 150 years and were highly seasonal, particularly during the period before industrialization, beginning in the mid-1800s (Figure 9). Annual average ice concentrations at Act2 reached a peak of $>12.5\ \mathrm{ng\,g^{-1}}$ in 1908 before beginning a general, though erratic, decline through the late 1940s, followed by a sharp drop in 1952, as can be seen in the annual data in Figure 9e. *McConnell et al*. [2007] have estimated BC atmospheric industrial emissions, concluding that the majority of industrial BC deposited in central Greenland probably came from North American emissions (at least during the period of high BC deposition from 1850 to 1951). The negative BC trend of 1951 onward, as has been found in the core record, suggests that long-range transport from Asia may not play an important role at these sites.

3.2.2. Model Simulation

[24] The models simulate that most of the precipitation falls as snow at the three sites, except at Act2 where 5% of the annual precipitation falls as rain. All models simulate similar snow rates of 0.1 mm/day at Humboldt, 0.8 mm/day at D4, and 0.6 mm/day at Act2 with no temporal trend. At Act2, the microphysical model MATRIX shows comparable BC deposition at PD, while the bulk model TCADI is too high. All models, but especially MATRIX, fail to match the high deposition rates of the early twentieth century. In addition, both models fail to reproduce the interannual variability measured in the ice cores throughout the historical period. This clearly points to the emission inventories used, which are mean decadal fluxes, linearly interpolated between the decades, which smoothens out any strong interannual variability caused by, e.g., intense biomass burning over some years.

[25] In the other two ice cores, D4 and Humboldt, the picture is similar, with one notable difference: the absence of the strong BC peak at the beginning of the twentieth century. The TCADI models appear to nicely calculate the Arctic Humboldt measurements but with less variability. This is also true for the period from 1890 to 1950 at D4, and less so in Act2. In the latter two cases, the BC decrease around 1950 is not captured. Since this decrease is not seen in Humboldt, we conclude that North American sources are responsible for the drop. North American emissions from land clearing and biofuel consumption of the domestic sector present a threefold decrease between 1910 and 1960 (Figure 7), whereas the measured BC deposition at Act2 shows an eightfold decrease. Despite the threefold decrease of the North American emissions, the BC deposition flux is calculated to decrease by a mere factor of 2.

[26] The intramodel differences are less pronounced in their sulfate simulation (Figures 9b, 9d, and 9f). All models nicely capture the measured trends but underestimate the extent of the interannual variability. Both models and measurements, at all locations, present an increasing sulfate deposition trend throughout the twentieth century and up to the 1970s, when a

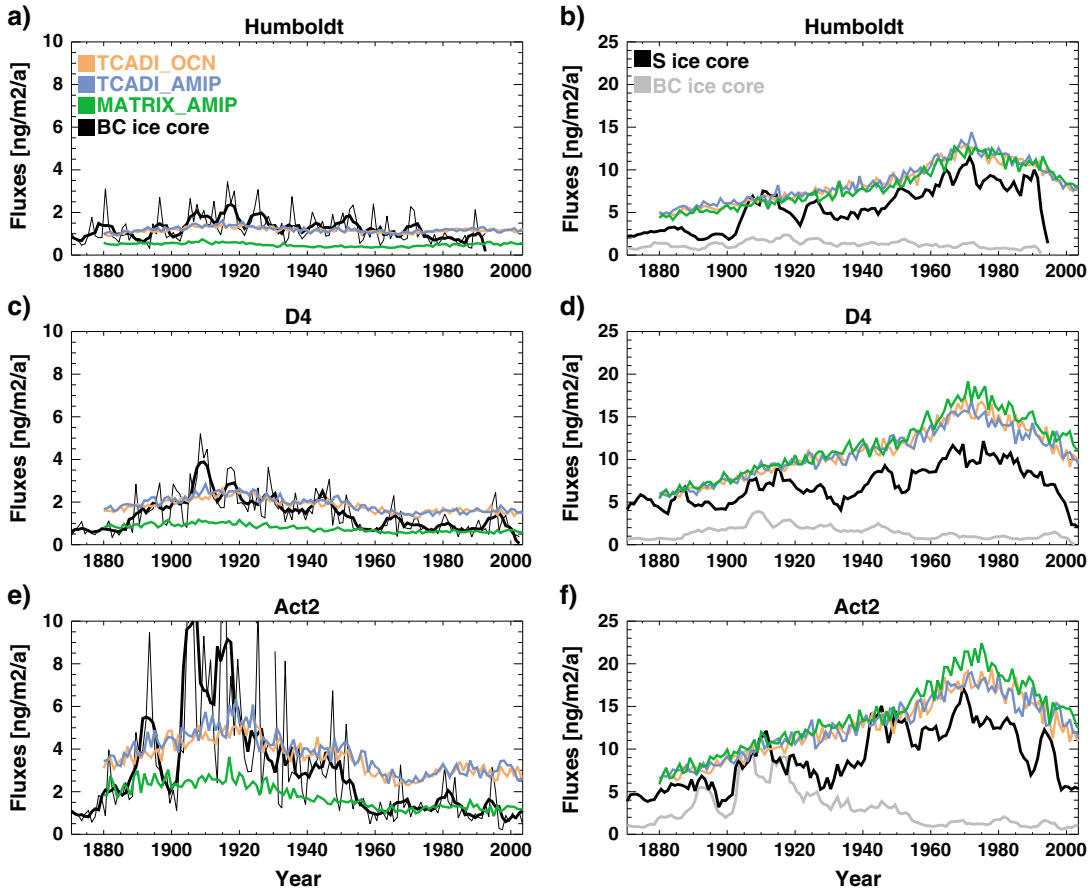

Figure 9. Refractory (left) black carbon and (right) sulfur time series at the Greenland stations. Ice core data (black) for 1850–2001 and model data. Annual (thin line) and 5 year mean (thick line) ice core measurements (black) and TCADI_OCN (orange), TCADI_AMIP (blue), and MATRIX_AMIP (green) simulations. Measured BC fluxes (the black lines from the left panels) are also plotted as grey lines in the right panels for reference.

decreasing trend appears. The models reproduce well the trends at all stations, but the absolute deposition is consistently higher by ~25% throughout the historical period. As in the case of BC, sulfate deposition decreases when moving from south to north, maximizing around 1970 at 15, 10, and 8 ng/m^2/a at Act2, D4, and Humboldt, respectively. The ice core records show increased concentrations around 1910, which are not reproduced by the models and therefore are lacking in the inventory. The underestimation of BC and SO_2 in the early twentieth century points to a missing source in the inventory.

3.3. Tibetan Plateau

3.3.1. Observed Trends in Ice Core Records

[27] Ice cores were extracted from several locations on the Tibetan Plateau (Figure 5c), covering the time period from 1950 to 2005: Mount Muztagh Ata (75.10°E, 38.28°N, 6300 m), Noijin Kangsang glacier (90.20°E, 29.04°N, 5950 m), and Zuoqiupu glacier (96.92°E, 29.21°N, 5600 m). BC and OC were measured on filters using the IMPROVE thermal/optical reflectance protocol [*Chow et al.*, 2004]. The interpretation of the measured time series is very complicated at these locations. The Tibetan glaciers are melting rapidly and are surrounded by the strongest anthropogenic emission sources and fastest growing regions on the planet: Southeast Asia and India. Due to its steep topography, the stations are affected by a range of meteorological systems. Zuoqiupu and Noijin Kangsang glaciers receive most of their precipitation by the Indian Monsoon, while Mount Muztagh Ata, located in the northwestern part of the Tibetan Plateau, is associated mainly with the westerly jet stream, which moves southward toward the Himalayas in winter [*Xu et al.*, 2009]. BC and OC time series are characterized by high deposition in the 1950s–1960s with a decreased deposition on the northwestern and central plateau in the 1960s and an overall increasing deposition at Zuoqiupu. *Xu et al.* [2009] attributed the high deposition in 1960 to European sources, despite the large distance. Newly performed measurements at the Muztagh Ata location, using the SP2 method, do not confirm a high BC concentration during the 1950s–1960s. The BC concentration in the new, not yet published, ice core is a factor of 10 lower compared to BC concentration derived by the thermal/optical reflectance protocol. In this paper, we will discuss the measurements as published by *Xu et al.* [2009]. However, we have to keep in mind the potentially large errors that can be caused by the measurement techniques.

3.3.2. Model Simulations

[28] The BC deposition levels between 1970 and 2005, 18 mg/m^2/a in Muztagh Ata, 12 mg/m^2/a in Zuoqiupu, and 6 mg/m^2/a in at Noijin Kangsang, are well captured by the models (Figure 10), as are some elements of the time evolution,

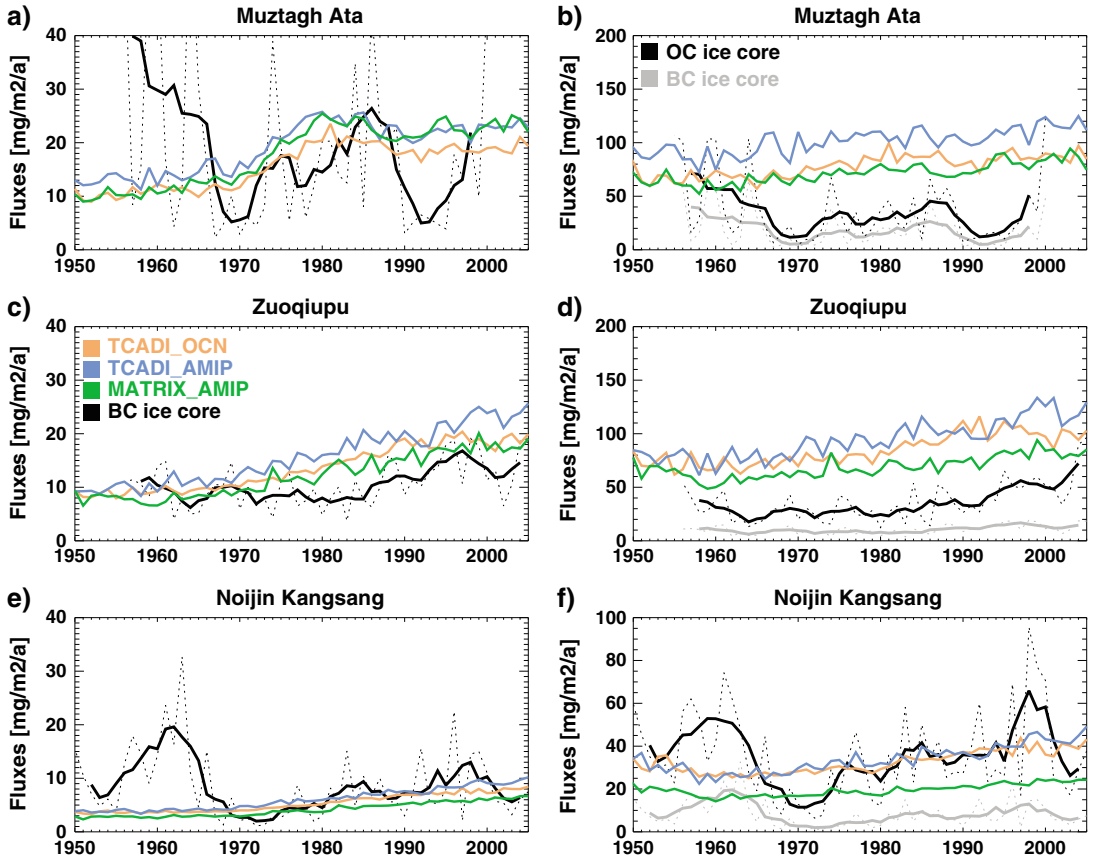

Figure 10. As Figure 6 but for ice core records from the Himalayas. The left panel shows BC deposition and the right panel organic carbon deposition fluxes. Measured BC fluxes (the black lines from the left panels) are also plotted as grey lines in the right panels for reference.

such as the observed increase at Zuoqiupu and the increase from 1970 to the present at Noijin Kangsang. However, the high deposition fluxes at Noijin Kangsang and Muztagh Ata around 1960 have not been reproduced. This discrepancy could be caused by the thermal/optical measurement technique, as the new SP2-measured ice core at Muztagh Ata does not confirm these results (B. Xu, personal communication, 2013). The trend in the SP2-measured ice cores matches the modeled trends; however, the absolute concentration levels are a magnitude lower. This discrepancy can be partly caused by the fact that the filter method measures all particles that got collected on the filter, whereas the optical SP2 method only detects particles with mass equivalent diameters above 60 nm. However, the large differences in the BC trends in the Muztagh Ata ice cores need to be further investigated by the measurement team. The regional emission sources (Figure 7) of India and Southeast Asia show strong increases since the 1960s, strongly driven by the domestic and industrial sectors. However, any evidence to support the high deposition in the midtwentieth century is lacking. European emissions peaked during this time, but the amplitude of the emissions is not able to explain the high concentrations in the ice core around 1960.

[29] Modeled aerosol types (Figure 8c) show that BC aerosols at Muztagh Ata are primarily anthropogenic with almost half of the present-day deposition being fresh BC. The ice cores additionally reported historical OC concentrations (Figure 10). The OC:BC ratios can give us an idea about possible sources. OC is calculated to increase, but BC increases faster than OC in all three locations, resulting in a decreasing trend in the OC:BC ratio. This does not agree with measurements, where they all present a very stable OC:BC ratio of roughly 2 throughout the whole period at Muztagh Ata, and 4–5 at the other two stations. The model simulations present a close-to-linear decrease of the ratio from 7 to 5 in Muztagh Ata and from 8 to 5 in the other two locations, between 1950 and 2010. Since the models generally agree pretty well with measurements, the reason of this discrepancy, if not due to measurement technique, should be in the OC simulation; the model is lacking an OC source, which can be related either with a missing (or underestimated) primary source or an underestimation of secondary organic aerosol (SOA) production. The latter is possibly underestimated in the region, since (a) the model does not include SOA formation from anthropogenic precursors, which increase when moving from PI to PD, and (b) all models are known to underestimate the anthropogenically enhanced natural SOA [*Spracklen et al.*, 2011].

[30] The time series at the Tibetan Plateau show differences among the aerosol schemes, with MATRIX generally showing lower BC and OC deposition rates. In the case of BC, this is caused by faster aging of aerosols in the microphysical scheme, but in the case of OC, we deal with different aging calculations (externally (TCADI) versus internally (MATRIX) mixed particles) and different OA sources. OA aging time scales in TCADI are ~7 days, whereas MATRIX has 4.5 days (Table 1). However, we also see differences

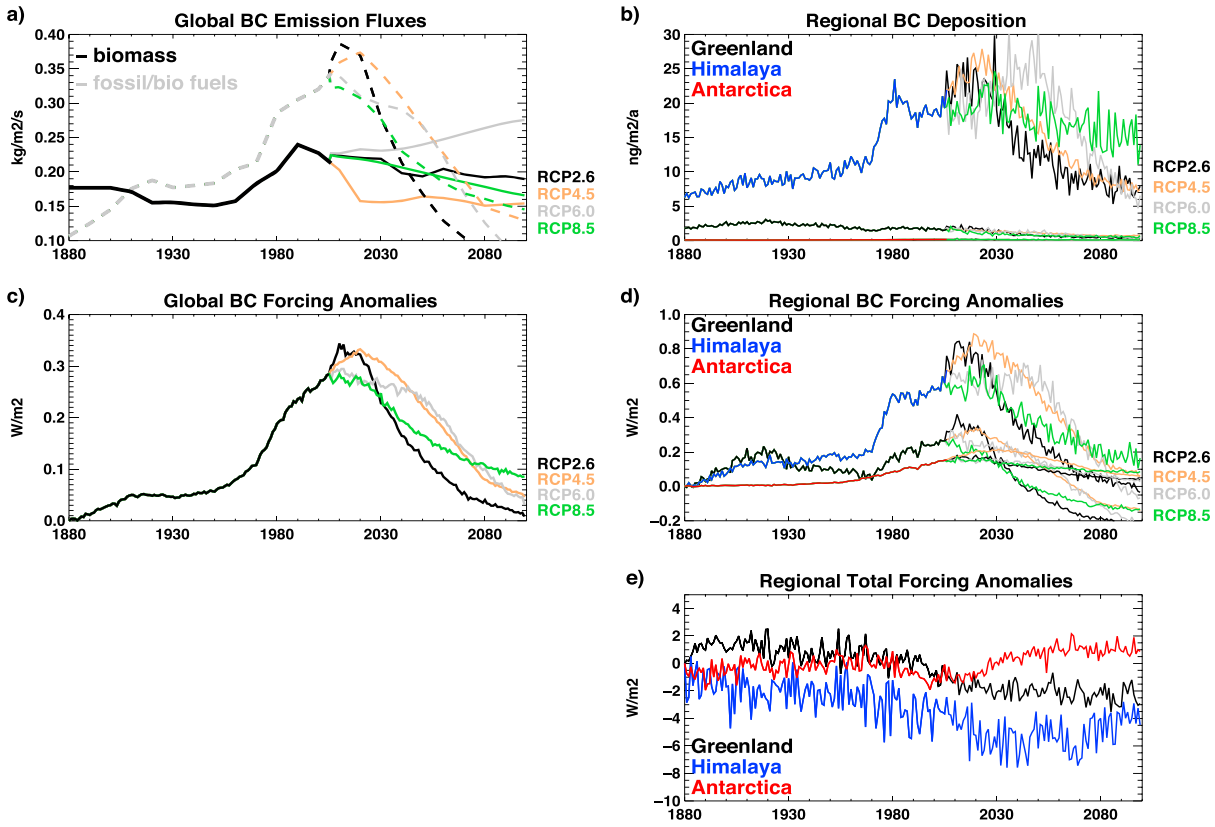

Figure 11. Time series of the TCADI_OCN model from 1880 to 2100 are shown for the historic simulation and the four future RCP projects. The panels show the global time series of (a) BC emissions and (c) BC forcing. Regional maps show (b) BC deposition, (d) BC forcing, and (e) total forcing at the three different stations: Law Dome, Antarctica (red), ACT2 in Greenland (black), and Muztagh Ata in the Himalayas (blue). Only RCP4.5 is shown in (e) for clarity.

among the two TCADI model versions in regard to ocean couplings, which relate to the ITCZ shift and its impact on tropical precipitation, a fact that was not important for the polar stations. Still, these differences are smaller than the TCADI-MATRIX differences and even smaller than the model-measurement differences. This indicates that the natural variability in the model is not as important as the aerosol source.

4. Future BC Deposition Fluxes and Radiative Forcing

[31] A set of four future scenarios, following the CMIP5 Representative Concentration Pathways (RCP2.6, RCP4.5, RCP6.0, and RCP8.5) [*van Vuuren et al.*, 2011], has been performed with the coupled ocean model (TCADI_OCN) for the 2006–2100 period. The four RCPs reflect the range of year 2100 radiative forcing values from 2.6 to 8.5 W/m^2, respectively. The net forcing is determined by forcings from greenhouse gases and aerosols, though the dominant factor across the scenarios is the forcing from CO_2. We will omit any discussion about the likelihood of these scenarios but note that most short-lived anthropogenic emission scenarios assume a steady decrease in all future aerosol emissions, due to different degrees of mitigation.

[32] In this section, we propose to analyze BC deposition fluxes and radiative forcings as predicted in the four RCPs. Figure 11b shows BC deposition rates at a station in each region: Antarctica (Law Dome), Greenland (Act2), and Tibet (Muztagh Ata). BC deposition in Greenland is about 10 times larger than in Antarctica and 10 times lower than in Tibet. Under most scenarios, BC deposition is projected to decline in the Himalayas after 2020 but remains at 1990 levels for RCP 8.5. Global BC instantaneous forcing anomalies (relative to the year 1880) (Figure 11c) follow the global BC emission trends (Figure 11a). Due to the global projections of future reductions in fossil fuel consumption, BC radiative forcing is projected to reach 1880 values by the end of the century in the most optimistic scenario RCP 2.6. Station BC forcing anomalies (Figure 11d) for the Himalayas and the Antarctic show similar trends compared to the global forcing. In Greenland, which is mostly influenced by North American emissions, the model simulates future BC forcings below 1880 values. This is caused by the assumption that North American BC was higher in 1880 than today and future scenarios assume even further reductions in BC emissions.

[33] The presence of carbonaceous aerosols in snow and ice alters the surface albedo and thereby changes the surface radiative forcing. Here we examine the global and regional

radiative forcing from BC aerosol surface albedo changes on land and sea ice. We calculate that the global radiative forcing (RF) decreases by 0.02 W/m^2 from 1850 to 2100 in RCP4.5. Specifically, the snow albedo forcing increases from 1850 to 1910 (globally, except in parts of Canada and China), remains fairly constant from 1910 to 1980 (with small increases in Asia and small decreases in North America and Europe), and decreases (worldwide) after 1980. The increases in RF from 1850 to 1900 are caused solely by anthropogenic emissions, since biomass burning emissions are constant during that period in the model. The maximum snow albedo RF of ~0.06 W/m^2 occurs around 2000. All RCP scenarios show similar trends after 2005, with RF values ranging from 0.012 to 0.021 W/m^2 in 2100 (RCP 8.5 and 2.6, respectively). In Antarctica, the radiative forcing from BC albedo changes is very low but relatively stable from 1850 to 2100. In the Arctic, the surface forcing decreases overall by 0.08 W/m^2 from 1850 to 2100. Interestingly, the trend exactly matches that of the global albedo RF, albeit greater in magnitude. The peak forcing in the Arctic (~0.24 W/m^2) occurs around 1980. In the Himalayas, the BC snow albedo forcing decreases slightly by 0.25 W/m^2 from 1850 to 2100. Forcing values are constant from 1850 to 1960, increase by 0.7 W/m^2 from 1960 to 2020, and decrease by approximately the same amount from 2020 to 2100. The maximum snow albedo forcing (~1.5 W/m^2) occurs around 2020.

[34] In order to put the BC forcing numbers into perspective, we present the regional total forcings in Figure 11e. The total instantaneous forcing is reacting to the greenhouse gas and short-lived species forcings, including those of CO_2, CH_4, C_2F_6, CF_4, N_2O, HFCs, ozone, and aerosol species (such as sulfates, nitrates, black and organic carbon, mineral dust, and sea salt), with additional effects from water vapor and cloud changes. The regional forcing anomalies (Figure 11e) show a decrease over time at Greenland and the Himalayas and a slight decrease in forcing at Antarctica between 1880 and 2005, with a slight increase in forcing that develops into the future. Note that, for clarity, only the RCP 4.5 scenario is presented. The regional forcing anomalies in Antarctica show a negative trend starting from 1980 and turning back into a positive forcing in the future projection. This is caused by the strong ozone forcing in Antarctica, which is related to an ozone depletion event that lasts for about 40 years [*Shindell et al*., 2013]. The forcing in Greenland shows positive forcing until ~1990 and then turns into a negative forcing that continues until the end of the simulation in 2100. In Greenland, the negative forcing is mostly driven by an increase in clouds in the Arctic. The planetary forcing trend in the Himalayas, in the Muztagh Ata mountain region, shows a rather strong (up to ~5 W/m^2) negative forcing trend, which is also caused by an increase in high clouds over the local region.

5. Conclusions and Perspectives

[35] Black carbon aerosol plays a unique and important role in the Earth's climate system [*Bond et al*., 2013]. In order to understand the role of BC in our climate system, climate models need to be able to simulate present and historic BC distributions. Ice and sediment core measurements provide a unique chance to evaluate historic concentrations. Improving the estimates on preindustrial black carbon concentrations is very important to support the current discussions on mitigation of short-lived climate forcers. Only by understanding the recent history of the atmosphere's chemical composition can we determine the level of influence that anthropogenic activities have on climate.

5.0.1. How Well Can We Constrain Current BC Residence Times?

[36] Although globally averaged aerosol residence times summarize effects of numerous processes including transformation, transportation, and removal, they provide a simple measure for model intercomparisons if similar emission inventories are used. CMIP5 models report BC lifetimes spanning from 3.9 to 15.2 days, with an average lifetime of 7.4 days [*Lee et al*., 2012]. The shortest lifetime of 3.9 days, as is also predicted by MATRIX, was reported by the NCAR-CAM5.1 model [*Liu et al*., 2012]. Our study demonstrated that 4 days is a realistic BC residence time under present-day conditions while using the CMIP5 inventory. GISS's microphysical aerosol scheme MATRIX was capable of predicting the correct BC lifetime in the Northern Hemisphere. However, residence times seemed to be too long for the Southern Hemisphere, as is evident in Antarctic ice core records. One model (TCADI) indicated that BC residence times may depend on aerosol source types, and therefore cloud change with time. However, neither the microphysical model nor the measurements supported that theory. The fact that there is no trend in BC deposition in the Antarctic demonstrated that remote background conditions were not affected by increased fossil fuel emissions. Aerosol solubility and aging in the GISS bulk aerosol model can be simply adjusted to more realistic values that would be below the currently used aging turnover time of 2.7 days and biomass burning BC solubility of 60%.

[37] Residence time, as pointed out earlier, averages transport and removal processes. All assumptions drawn here are in reference to the used emissions. We discussed the differences caused by two aerosol schemes, but we must also keep in mind that we used the same host model in all experiments. Turbulent and convective transport processes play a crucial role for aerosol lifetime. Unfortunately, these processes cannot yet be evaluated with observations, but future campaigns should address this source of large model uncertainties.

5.0.2. How Well Can We Simulate Historic Concentrations of the Past 150 Years?

[38] After having demonstrated that MATRIX provides a decent present-day BC simulation, while TCADI shows good near-surface concentrations in the United States but overestimates upper tropospheric concentrations by a factor of 2, testing the simulations over the past 150 years mainly informs us about the historic emission inventory. With respect to aerosol emissions, we conclude that early twentieth century North American emissions, and possibly midcentury Eastern European emissions, are most likely greatly underestimated in the emission inventory [*Lamarque et al*., 2010]. This bias has consequences when calculating aerosol-related forcings if IPCC definitions [*IPCC*, 2007] such as preindustrial versus present-day forcing changes are used as a basis. Ice core measurements are proof that these definitions only give a poor description of anthropogenic carbonaceous aerosol forcings, due to the large uncertainties relating to preindustrial aerosol levels. Carbonaceous emissions have been linked with human

settlement long before industrialization due to land cover change and wood burning activities. For example, BC emissions in the United States have been higher in 1850 than at present day. A better definition of anthropogenic forcing would take into account all human-induced activities, independent from its preindustrial concentrations.

5.0.3. What are the Future BC Deposition Fluxes at the Three Ice Caps Following the Four CMIP5 RCP Scenarios?

[39] The future scenarios show further increases in BC deposition on the Himalayan glaciers. The Antarctic stations are remote enough to not be influenced by past or future aerosol trends, and in Greenland, we see further decreasing BC trends due to decreasing North American BC emissions in the CMIP5 projections. The most alarming impacts are thus the fast growing Asian emissions and their influence, in combination with a warming climate and the already retreating glaciers of this region.

[40] In this study, we used the ice core data primarily to evaluate our model, test the emission inventory, understand some of the observed features, and ultimately use the model to predict future concentrations and forcings. We discovered interesting details that invite further studies to fully understand ice core data sets. Such studies would include the following: (a) improved historical emission estimates, especially regarding Russia, Asia, and early twentieth century North American emissions; (b) an evaluation of biomass burning emissions that respond to climate change, in order to understand climate variability and aerosol feedbacks; (c) near- and far-source evaluations of carbonaceous aerosols, to further understand aerosol transport, aging effects, and residence times; (d) an examination of Monsoon circulation shifts caused by climate change and impacts on aerosol transport; and (e) an investigation of the differences in thermal/optical and soot photometric measurement techniques on the Tibetan ice cores.

Appendix A

A1. Model Description

[41] The climate model used in this study is the NASA GISS climate model, ModelE2 (denoted GISS-E2-R in the CMIP5 archive) with 2° by 2.5° horizontal resolution and 40 vertical layers, having the model top at 0.1 hPa. The TCADI model runs analyzed here are part of the CMIP5 data archive. A detailed model description and evaluation of the present-day climate simulations are reported in Schmidt et al. (in preparation, 2013).

A1.1. Aerosol Schemes

[42] The bulk aerosol scheme, TCADI, is a mass-based aerosol scheme. TCADI interactively calculates aerosol species such as sulfate [*Koch et al*., 2006, 2007], nitrate [*Bauer et al*., 2007a], elemental and organic carbon, sea salt [*Koch et al*., 2006], and dust [*Miller et al*., 2006]. This scheme also includes heterogeneous chemistry on dust surfaces [*Bauer and Koch*, 2005; *Bauer et al*., 2007b] and SOA production [*Tsigaridis and Kanakidou*, 2007]. The mass per aerosol species is tracked, and a fixed size, density, and solubility are assigned per transported tracer, except for dust where inorganic coatings influence solubility. We will give some more specifics here about BC because of its relevance for this study. BC is tracked with three tracers all having the same size (0.1 μm radius) and density (1300 kg/m^3), but differences in solubility. BC from biomass burning sources is assumed to have a constant 60% solubility. Energy-related BC is assumed to initially be hydrophobic and then age to become hydrophilic with an e-fold lifetime of 2.7 days.

[43] The microphysical aerosol scheme, MATRIX [*Bauer et al*., 2008, 2010; *Bauer and Menon*, 2012], is based on the quadrature method of moments [*McGraw and Wright*, 2003]. MATRIX dynamics include nucleation, new particle formation, particle emissions, gas-particle mass transfer, aerosol phase chemistry, condensational growth, coagulation, and cloud activation. The model tracks mass and number concentrations of 16 aerosol populations, defined by mixing state. BC is present in 7 of the 16 populations and its definitions are as follows: BC with ≤5% inorganic coatings (inorganic coatings can be comprised out of sulfate, nitrate, and ammonia), BC with 5–20% inorganic coatings, BC with ≥20% inorganic coatings, BC-dust (including inorganic coatings), BC and organics (including inorganic coatings), BC and sulfate (coagulated, including inorganic coatings), and BC mixed with everything (including dust and sea salt). Size, density, and solubility of each population are calculated prognostically. The averaged solubility per aerosol population in MATRIX is calculated by using a volume-weighted approach, depending on the chemical composition of each population.

A1.2. Deposition

[44] Both aerosol schemes, TCADI and MATRIX, use the same parameterizations for dry-, wet-, and BC on ice deposition, but due to the fact that the microphysical properties of the aerosols are calculated differently, the removal rates differ substantially.

[45] Turbulent dry deposition is based on the resistance-in-series scheme described in *Koch et al*. [1999]. The scheme is coupled to the model boundary layer scheme of the GCM and depends on the mean diameter of the aerosol population. Gravitational settling depends on the aerosol population mean diameter and density and accounts for the effects of RH on density and size. The wet deposition schemes are described in *Koch et al*. [1999, 2006]. The model treats two types of clouds, convective and stratiform clouds. Tracer treatment in clouds follows the cloud processes, so that tracers are transported, dissolved, evaporated, and scavenged (with cloud-water autoconversion and by raindrop impaction beneath clouds). This parameterization requires information about aerosol size, density, and solubility, which are calculated for each aerosol population by MATRIX and are constant per tracer in TCADI.

[46] Both models calculate BC deposition on ice and snow surfaces and determine the impact on albedo as described in *Koch and Hansen* [2005]. To represent BC deposition on frozen surfaces and modifications to snow/ice albedo, BC concentrations in the top layer of snow (on land and sea ice) are used to calculate the albedo reduction on snow grains with sizes varying from 0.1 to 1 mm [*Koch et al*., 2009].

A2. Model Setup

[47] We analyze historical simulations from 1850 to 2005, which consider both anthropogenic and natural forcings. The anthropogenic forcings include time-varying well-mixed

GHGs, ozone (O_3), tropospheric aerosols, stratospheric water vapor from methane oxidation, a parameterized indirect effect of aerosols on clouds, soot effect on snow and ice albedos, and land use changes. Natural forcings arise from changing volcanic aerosols, solar irradiance, and Earth orbital parameters. The ensemble of five historical simulations with the coupled climate model uses initial conditions at intervals of 20 years of the control experiment, which allows for the accounting of unforced model variability. The control run is integrated with constant forcings corresponding to the year 1850.

A2.1. Oceans

[48] The "Russell ocean model" is described by *Russell et al*. [1995]. This ocean model is a mass-conserving dynamic ocean model with a horizontal resolution of 1.25° longitude by 1° latitude, and it has 32 vertical levels with finer resolution at the top 100 m. The model uses C-grid for the momentum equations. The ocean model includes the K-Profile Parameterization (KPP) parameterization for vertical mixing [*Large et al*., 1994] and the Gent-McWilliams parameterization for mixing effect associated with mesoscale eddies [*Gent and McWilliams*, 1990]. We employ no flux correction in the heat exchange between the atmosphere and the ocean.

[49] We also carried out historical simulations with the identical atmospheric model in the so-called AMIP configuration, which uses observed sea surface temperature (SST) and sea ice (SI). The five-member ensemble was run for 1880–2010 with SST, SI, and varying climate forcings. Each ensemble member is started with a perturbed initial state of the atmospheric conditions.

A2.2. Future Scenarios

[50] A set of four future emission scenarios, the so-called Representative Concentration Pathways (RCPs: RCP2.6, RCP4.5, RCP6.0, and RC P8.5), developed as a basis for long-term and short-term modeling experiments [*van Vuuren et al*., 2011], has been performed for TCADI_OCN. Each of the RCPs covers the 2006–2100 period starting as a continuation of the historical simulations. The four RCPs reflect the range of year 2100 radiative forcing values from 2.6 to 8.5 W/m^2 and are named accordingly. The net forcing is determined by both positive forcing from greenhouse gases and negative forcing from aerosols though the dominant factor across the scenarios is the forcing from CO_2. Radiative forcings from the land use scenarios are relatively small compared to radiative forcings from greenhouse gases, although deforestation is an important element in the CO_2 emissions. All simulations are coupled to the gas-phase chemistry scheme G-PUCCINI, documented in *Shindell et al*. [2006]. Sea salt and dust emission fluxes are calculated interactively. Additional natural and anthropogenic fluxes are provided by the CMIP5 emissions inventory [*Lamarque et al*., 2010]. We carried out the ensemble of five runs for the RCP4.5 scenario, while for the three other RCP experiments, we conducted single runs for the 21st century.

[51] **Acknowledgments.** This work has been supported by the NASA MAP program Modeling, Analysis and Prediction Climate Variability and Change (NN-H-04-Z-YS-008-N and NN-H-08-Z-DA-001-N). Resources supporting this work were provided by the NASA High-End Computing (HEC) Program through the NASA Center for Climate Simulation (NCCS) at Goddard Space Flight Center. We acknowledge the IMPROVE monitoring program. We acknowledge the use of HIPPO data products (http://www.eol.ucar.edu/projects/hippo/). The HIPPO mission was funded by NSF, NOAA, and NASA.

References

Bauer, S. E., and D. Koch (2005), Impact of heterogeneous sulfate formation at mineral dust surfaces on aerosol loads and radiative forcing in the Goddard Institute for Space Studies general circulation model, *J. Geophys. Res.*, *110*, D17202, doi:10.1029/2005JD005870.

Bauer, S. E., D. Koch, N. Unger, S. M. Metzger, D. T. Shindell, and D. G. Streets (2007a), Nitrate aerosols today and in 2030: A global simulation including aerosols and tropospheric ozone, *Atmos. Chem. Phys.*, *7*(19), 5,043–5,059.

Bauer, S. E., M. I. Mishchenko, A. A. Lacis, S. Zhang, J. P. Perlwitz, and S. M. Metzger (2007b), Do sulfate and nitrate coatings on mineral dust have important effects on radiative properties and climate modeling?, *J. Geophys. Res.*, *112*, D06307, doi:10.1029/2005JD006977.

Bauer, S. E., D. L. Wright, D. Koch, E. R. Lewis, R. McGraw, L. S. Chang, S. E. Schwartz, and R. Ruedy (2008), MATRIX (Multiconfiguration Aerosol TRacker of mIXing state): An aerosol microphysical module for global atmospheric models, *Atmos. Chem. Phys.*, *8*(20), 6,003–6,035.

Bauer, S. E., S. Menon, D. Koch, T. C. Bond, and K. Tsigaridis (2010), A global modeling study on carbonaceous aerosol microphysical characteristics and radiative effects, *Atmos. Chem. Phys.*, *10*(15), 7,439–7,456.

Bauer, S. E., and S. Menon (2012), Aerosol direct, indirect, semidirect, and surface albedo effects from sector contributions based on the IPCC AR5 emissions for preindustrial and present-day conditions, *J. Geophys. Res. Atmos.*, *117*.

Bisiaux, M. M., R. Edwards, J. R. McConnell, M. R. Albert, H. Anschutz, T. A. Neumann, E. Isaksson, and J. E. Penner (2012a), Variability of black carbon deposition to the East Antarctic Plateau, 1800–2000 AD, *Atmos. Chem. Phys.*, *12*(8), 3,799–3,808.

Bisiaux, M. M., R. Edwards, J. R. McConnell, M. A. J. Curran, T. D. Van Ommen, A. M. Smith, T. A. Neumann, D. R. Pasteris, J. E. Penner, and K. Taylor (2012b), Changes in black carbon deposition to Antarctica from two high-resolution ice core records, 1850–2000 AD, *Atmos. Chem. Phys.*, *12*(9), 4,107–4,115.

Bond, T. C., et al. (2013), Bounding the role of black carbon in the climate system: A scientific assessment, *J. Geophys. Res.*, *118*, 5,380–5,552, doi:10.1002/jgrd.50171.

Chow, J. C., J. G. Watson, L. W. A. Chen, W. P. Arnott, and H. Moosmuller (2004), Equivalence of elemental carbon by thermal/optical reflectance and transmittance with different temperature protocols, *Environ. Sci. Technol.*, *38*(16), 4,414–4,422.

Flanner, M. G., C. S. Zender, J. T. Randerson, and P. J. Rasch (2007), Present-day climate forcing and response from black carbon in snow, *J. Geophys. Res.*, *112*, D11202, doi:10.1029/2006JD008003.

Gent, P. R., and J. C. McWilliams (1990), Isopycnal mixing in ocean circulation models, *J. Phys. Oceanogr.*, *20*(1), 150–155.

Hansen, J., and L. Nazarenko (2004), Soot climate forcing via snow and ice albedos, *Proc. Natl. Acad. Sci. U.S.A.*, *101*(2), 423–428.

IPCC, (2007) Climate Change (2007), The Physical Science Basis. *Contribution of Working Group I to the Fourth Assessment Report of the Intergovernmental Panel on Climate Change*, edited by S. Solomon, D. Qin, M. Manning, Z. Chen, M. Marquis, K. B. Averyt, M. Tignor, and H. L. Miller, Cambridge University Press, Cambridge, United Kingdom and New York, NY, USA.

Koch, D., D. Jacob, I. Tegen, D. Rind, and M. Chin (1999), Tropospheric sulfur simulation and sulfate direct radiative forcing in the Goddard Institute for Space Studies general circulation model, *J. Geophys. Res.*, *104*, 23,799–23,822, doi:10.1029/1999JD900248.

Koch, D., and J. Hansen (2005), Distant origins of Arctic black carbon: A Goddard Institute for Space Studies ModelE experiment, *J. Geophys. Res.*, *110*, D04204, doi:10.1029/2004JD005296.

Koch, D., G. A. Schmidt, and C. V. Field (2006), Sulfur, sea salt and radionuclide aerosols in GISS ModelE, *J. Geophys. Res.*, *111*, D06206, doi:10.1029/2004JD005550.

Koch, D., T. C. Bond, D. Streets, N. Unger, and G. R. van der Werf (2007), Global impacts of aerosols from particular source regions and sectors, *J. Geophys. Res.*, *112*, D02205, doi:10.1029/2005JD007024.

Koch, D., S. Menon, A. Del Genio, R. Ruedy, I. Alienov, and G. A. Schmidt (2009), Distinguishing aerosol impacts on climate over the past century, *J. Climate*, *22*(10), 2,659–2,677.

Kopacz, M., D. L. Mauzerall, J. Wang, E. M. Leibensperger, D. K. Henze, and K. Singh (2011), Origin and radiative forcing of black carbon transported to the Himalayas and Tibetan Plateau, *Atmos. Chem. Phys.*, *11*(6), 2,837–2,852.

Lamarque, J. F., et al. (2010), Historical (1850–2000) gridded anthropogenic and biomass burning emissions of reactive gases and aerosols: Methodology and application, *Atmos. Chem. Phys.*, *10*(15), 7,017–7,039.

Large, W. G., J. C. McWilliams, and S. C. Doney (1994), Oceanic vertical mixing: A review and a model with nonlocal boundary layer parameterization, *Rev. Geophys.*, *32*(4), 363–403.

Lee, Y. H., et al. (2012), Evaluation of preindustrial to present-day black carbon and its albedo forcing from ACCMIP (Atmospheric Chemistry and Climate Model Intercomparison Project), *Atmos. Chem. Phys. Discuss.*, *12*(8), 21,713–21,778, doi:10.5194/acpd-12-21713-2012.

Liu, X., et al. (2012), Toward a minimal representation of aerosols in climate models: Description and evaluation in the Community Atmosphere Model CAM5, *Geosci. Model Dev.*, *5*(3), 709–739.

McConnell, J. R. (2010), New Directions: Historical black carbon and other ice core aerosol records in the Arctic for GCM evaluation, *Atmos. Environ.*, *44*(21–22), 2,665–2,666.

McConnell, J. R., R. Edwards, G. L. Kok, M. G. Flanner, C. S. Zender, E. S. Saltzman, J. R. Banta, D. R. Pasteris, M. M. Carter, and J. D. W. Kahl (2007), 20th-Century industrial black carbon emissions altered arctic climate forcing, *Science*, *317*(5843), 1,381–1,384.

McGraw, R., and D. L. Wright (2003), Chemically resolved aerosol dynamics for internal mixtures by the quadrature method of moments, *J. Aerosol Sci.*, *34*(2), 189–209.

Miller, R. L., et al. (2006), Mineral dust aerosols in the NASA Goddard Institute for Space Sciences ModelE atmospheric general circulation model, *J. Geophys. Res.*, *111*, D06208, doi:10.1029/2005JD005796.

Pechony, O., and D. T. Shindell (2010), Driving forces of global wildfires over the past millennium and the forthcoming century, *Proc. Natl. Acad. Sci.*, *107*, 19,167–19,170, doi:10.1073/pnas.1003669107.

Russell, G. L., J. R. Miller, and D. Rind (1995), A coupled atmosphere-ocean model for transient climate change studies, *Atmos.-Ocean*, *33*(4), 683–730.

Schwarz, J. P., J. R. Spackman, R. S. Gao, L. A. Watts, P. Stier, M. Schulz, S. M. Davis, S. C. Wofsy, and D. W. Fahey (2010), Global-scale black carbon profiles observed in the remote atmosphere and compared to models, *Geophys. Res. Lett.*, *37*, L18812, doi:10.1029/2010GL044372.

Shindell, D. T., G. Faluvegi, N. Unger, E. Aguilar, G. A. Schmidt, D. M. Koch, S. E. Bauer, and R. L. Miller (2006), Simulations of preindustrial, present-day, and 2100 conditions in the NASA GISS composition and climate model G-PUCCINI, *Atmos. Chem. Phys.*, *6*, 4,427–4,459.

Shindell, D. T., et al. (2013), Interactive ozone and methane chemistry in GISS-E2 historical and future climate simulations, *Atmos. Chem. Phys.*, *13*, 2,653–2,689, doi:10.5194/acp-13-2653-2013.

Spracklen, D. V., et al. (2011), Aerosol mass spectrometer constraint on the global secondary organic aerosol budget, *Atmos. Chem. Phys.*, *11*(23), 12,109–12,136.

Tsigaridis, K., and M. Kanakidou (2007), Secondary organic aerosol importance in the future atmosphere, *Atmos. Environ.*, *41*(22), 4,682–4,692.

van Vuuren, D. P., et al. (2011), The representative concentration pathways: An overview, *Clim. Change*, *109*(1-2), 5–31.

Xu, B. Q., et al. (2009), Black soot and the survival of Tibetan glaciers, *Proc. Natl. Acad. Sci. U.S.A.*, *106*(52), 22,114–22,118.